XIV International Conference on Computational Plasticity. Fundamentals and Applications
COMPLAS 2019
E. Oñate, D.R.J. Owen, D. Peric , M. Chiumenti, and Eduardo de Souza Neto (Eds)

# MACROSCOPIC FE-SIMULATION OF RESIDUAL STRESSES IN THERMO-MECHANICALLY PROCESSED STEELS CONSIDERING PHASE TRANSFORMATION EFFECTS

**B.-A. BEHRENS, A. CHUGREEV AND C. KOCK***

Institut für Umformtechnik und Umformmaschinen (IFUM)
Leibniz Universität Hannover (LUH)
An der Universität 2, Garbsen 30823, Germany
*e-mail: kock@ifum.uni-hannover.de, web page: http://www.ifum.uni-hannover.de

**Key words:** thermo mechanical forming process, finite element analysis, residual stresses, phase transformation effects, transformation induced plasticity, X-ray diffraction.

**Abstract.** Residual stresses are an important issue as they affect both the manufacturing processes as well as the performance of the final parts. Taking into account the whole process chain of hot forming, the integrated heat treatment provided by a defined temperature profile for cooling of the parts offers a great potential for the targeted adjustment of the desired residual stress state. However, in addition to elastic, plastic and linear thermal strain components, the complex material phenomena arising from phase transformation effects of the polymorphic steels have to be considered in order to predict the residual stresses. These transformation strains account for the plastic deformation at the phase boundary between the emerging and the parent phase. In addition, they are strongly related to the transformation induced plasticity (TRIP) phenomena which depend on the stress state. The aim of this study is the investigation of TRIP effects and their impact on residual stresses regarding the typical hot forming steels 1.7225 (DIN: 42CrMo4) and 1.3505 (DIN: 100Cr6) by means of an experimental-numerical approach. The TRIP behaviour of the materials under consideration is integrated into an FE simulation model in the commercial software Simufact.forming for the purpose of residual stress prediction. The experimental thermo-mechanical investigations are carried out using a quenching and forming dilatometer. These experiments are numerically modelled by means of FEM which allows TRIP coefficients to be determined phase-specifically by numerical identification. For validation of the improved FE-model, an experimental thermo-mechanical reference process is considered, in which cylindrical specimens with an eccentric hole are hot formed and subsequently cooled by different temperature routes. Finally, the numerical model is validated by means of a comparison between residual stress states determined with X-ray diffraction and predicted residual stresses from the simulation.

## 1 INTRODUCTION

In metal forming, the arising residual stresses influence the material behaviour during and

after manufacturing as well as the performance of the final component [1]. In the past, the focus of forming process design was on minimizing or eliminating residual stresses. However, the residual stress can also serve to improve the properties of the components through targeted use, for example with regard to distortions or wear behaviour [2]. The cost-efficient virtual process design of individual process steps or even an entire process chain is gaining in importance due to economic globalization, continuously rising energy costs and growing competition in the manufacturing industry. Especially in the field of hot forming, process design in trial and error approaches represents a substantial cost and time expenditure [3]. At the same time, hot forming offers great potential for energy-efficient production of components by integrated heat treatment in the cooling phase after forming. The parameters of the forming process in combination with the temperature control over the entire process chain of the hot forming process result in many control parameters influencing the resulting residual stress condition. Nevertheless, the FE simulation-supported design of hot forming processes using polymorphic steels is very challenging. As shown in **FIGURE 1a**, numerous influencing parameters from thermal, metallurgical and mechanical fields exist, which affect each other in complex interactions [4, 5].

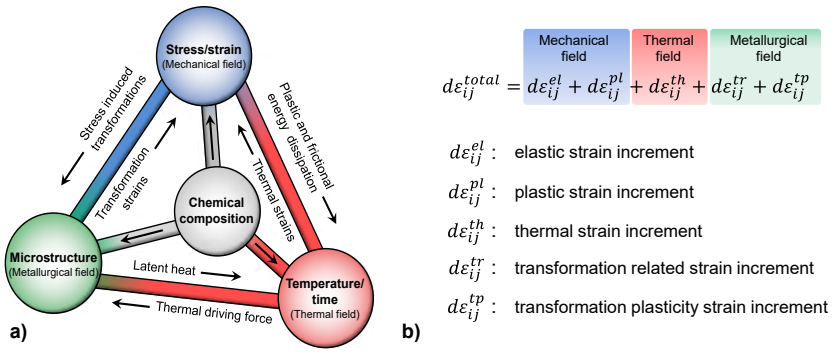


**Figure 1**: Interrelated thermo-mechanical-metallurgical material phenomena during thermo-mechanical processing of steel [6] (a); basic principles of the additive strain decomposition method (b).

For realistic process simulation, an appropriate mathematical model capable of consistently describing the polymorphic material behaviour is required. For this purpose, fully coupled thermo-mechanical-metallurgical FE-simulations based on the theory of additive strain decomposition method are often used in the literature [7, 8]. The components of such a method are structured in **FIGURE 1b** according to their physical origin. In addition to the elasto-viscoplastic strain increments and the thermal strain increments, transformation related strains occur due to the microstructural phase transformation. The transformation related strains are caused by volume changes due to different lattice constants of the parent and the emerging microstructural phase. In general, the transformation behaviour for calculation of transformation related strains is described by continuous-cooling-transformation (CCT) diagrams and time-temperature-transformation (TTT) diagrams. Thereby, CCT diagrams describe the transformation behaviour of the material during continuous cooling, whereas TTT diagrams represent the transformation behaviour after quenching and subsequent holding at a certain test temperature [9]. For phase transformation simulations TTT diagrams are required according to the mathematical approaches, while CCT diagrams provide a vivid diagram for reading the phase transformations occurring during continuous cooling. At a

given stress state, according to the definition of [10], an additional plastic strain increment in relation to the transformation related strains in the stress free state occurs, which is referred to as transformation plasticity (TRIP). The resulting strain composition acts as driving force for residual stresses and thermal distortions in the final components. The TRIP strains in particular have a special influence on the total strain and thus on the resulting residual stresses, since they are significantly dependent on the prevailing stress state. According to [11], there is a linear relationship between the applied mechanical stress and the TRIP strain. In addition, several authors [12, 13, 14] have shown that, besides the amount, the direction of the stresses also influences the magnitude of the TRIP strain. In the literature for the description of the transformation plasticity strain, a mathematical basic equation is assumed, which generally can be expressed as follows according to [15]:

$$\boldsymbol{d\varepsilon_{ij}^{tp}} = \frac{3}{2}\sum_{n=1}^{m} K_n f_n(\zeta_n) s \tag{1}$$

The total TRIP strain is calculated as the sum of the TRIP strains of the individual phases $n$, whereby $m$ is the total number of phases involved. The stress deviator is designated by $s$ and the factor $K_n$ is the material and phase specific coefficient of the transformation plasticity. Some authors have already reported values for the coefficient $K_n$ for the martensitic transformation. Hence, for 1.7225 $K = 4.2 \times 10^{-5}$ MPa$^{-1}$ [16] and for 1.5528 $K = 8.68 \times 10^{-5}$ MPa$^{-1}$ for tensile stresses and $K = 9.33 \times 10^{-5}$ MPa$^{-1}$ for compressive stresses [17], respectively, are indicated. The term $f_n(\zeta_n)$ denotes a monotonous function depending on the already transformed volume fraction of the emerging phase $\zeta_n$, whereby the conditions $f_n(\zeta_n = 0) = 0$ (start of transformation) and $f_n(\zeta_n = 1) = 1$ (end of transformation) must be satisfied. An outline of the approaches from the literature of this function is given in [18].

This article presents the design and validation of an FE-simulation model for the numerical investigation of residual stresses in hot forming processes regarding the materials 1.7225 (DIN designation: 42CrMo4 [19]) and 1.3505 (DIN designation: 100Cr6 [20]). In Section 2 particular emphasis is placed on the experimental investigation of phase transformation effects with respect to TRIP strains. A numerical study is used to determine the characteristic TRIP coefficients of the different microstructural phases in Section 3. Finally, a hot forming process is designed in the FE software Simufact.forming and the model is validated by experimental tests in Section 4.

## 2 MATERIAL CHARACTERISATION

### 2.1 Thermo-mechanical material data for hot forming simulation applications

As described introductory, extensive material data are required for the fully coupled simulation of a thermo-mechanical forming process. In order to simulate the hot forming step, information on the flow behaviour of the material at corresponding temperatures and strain rates must be available. For this purpose, flow curves of the investigated steels were determined by cylinder compression tests using the servo hydraulic forming simulator Gleeble 3800-GTC. The cylindrical samples had the dimensions Ø10 mm in diameter and

15 mm in height. The tests were performed at the relevant temperatures (900, 1000, 1100 and 1200 °C) with an equivalent plastic strain rate of 1 $s^{-1}$. In addition, the tests were carried out at a temperature of 1000 °C with the equivalent plastic strain rates of 10 $s^{-1}$ and 50$s^{-1}$. The determined flow curves are shown in **Figure 2**. For a continuous description of the flow stress $k_f$, multidimensional functions according to the approach of Hensel and Spittel [21] were calibrated with respect to equivalent plastic strain $\varepsilon_{eq}$, equivalent plastic strain rate $\dot{\varepsilon}_{eq}$ and temperature $T$. **Equation (2)** shows the formula for calculating the flow stress, with the regression coefficients ($A$, $m_1$, $m_2$, $m_3$, $m_4$) listed in **Table 1**.

$$k_f = Ae^{(m_1 T)}\varepsilon_{eq}^{m_2} e^{\frac{m_4}{\varepsilon_{eq}}}\dot{\varepsilon}_{eq}^{m_3} \tag{2}$$

**Table 1:** Parameters determined for the calculation of the flow stress $k_f$ of the considered steel alloys 1.7225 and 1.3505 according to [19].

| Material | $A$ [MPas] | $m_1$ [°C$^{-1}$] | $m_2$ [-] | $m_3$ [-] | $m_4$ [-] |
|---|---|---|---|---|---|
| 1.7225 | 3805 | -0.003458 | -0.1083 | 0.1497 | -0.04373 |
| 1.3505 | 2208 | -0.003068 | -0.179 | 0.1695 | -0.04383 |

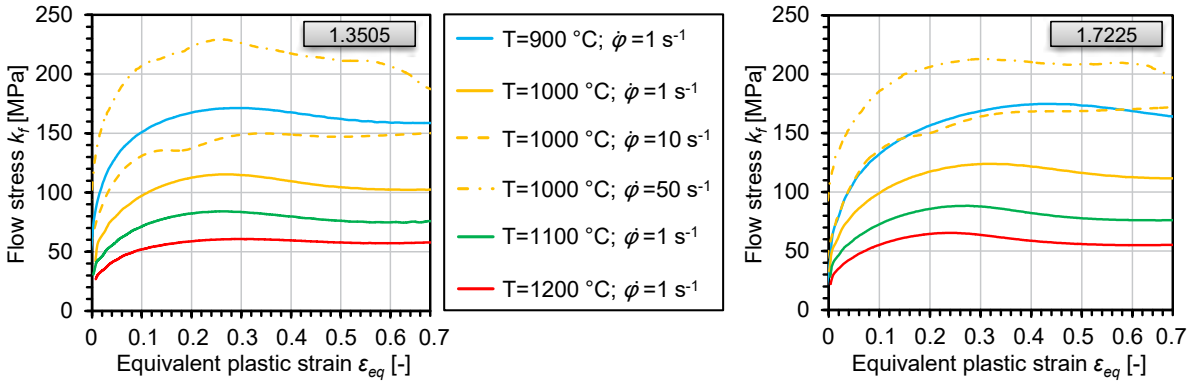


**Figure 2**: Determined flow curves of the investigated materials 1.7225 (left) and 1.3505 (right) for hot forming applications from the servo hydraulic forming simulator Gleeble 3800-GTC.

For the numerical modelling of the phase transformations during cooling from the forging heat, TTT diagrams of the examined materials were generated using an experimental-numerical approach. In order to visualise the phase transformations that occur during continuous cooling, CCT diagrams of the alloys are shown in **Figure 3**. More detailed information on the experimental-numerical procedure for analysing the phase transformation behaviour of the batches used in this study for the materials 1.7225 and 1.3505 can be found in [22].

Besides hot forming flow curves and TTT diagrams, further phase-specific material data such as specific heat capacity, latent heat or phase specific flow curves are required for thermo-mechanical process simulation. In most cases, it is difficult to generate experimental material data for pure microstructural phases [23]. For this reason, material data has been generated with the thermodynamic simulation software JMatPro [24] as an initial estimation. With help of this software, it is possible to generate mechanical and thermal material data by means of thermodynamic calculation approaches from [25] and [26] based on the chemical composition (see **Table 2**) of the steel alloys. Further details on the material data can be found in [27].

**Table 2:** Chemical composition of steel alloys 1.7225 and 1.3505 according to international standards [17, 18] used for material data generation with JMatPro.

| [wt%] | C | Si | Mn | P | S | Cr | Mo | Fe |
|---|---|---|---|---|---|---|---|---|
| 1.7225 | 0.42 | 0.25 | 0.75 | 0.025 | 0.035 | 1.10 | 0.22 | balance |
| 1.3505 | 0.99 | 0.25 | 0.35 | 0.025 | 0.015 | 1.475 | 0.10 | balance |

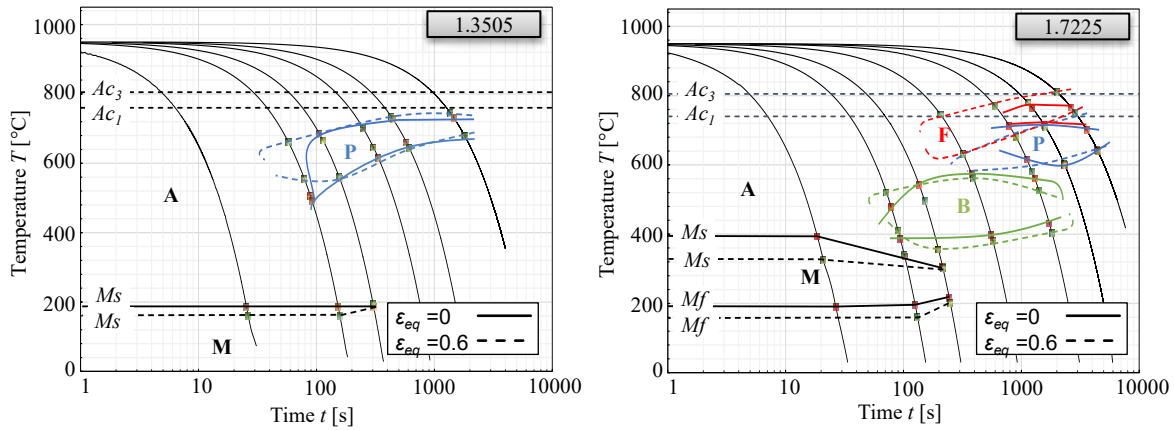


**Figure 3:** CCT-diagrams for the investigated materials 1.7225 (left) and 1.3505 (right) without and with a previous austenite deformation $\varepsilon_{eq}$.

## 2.2 Experimental study on the transformation induced plasticity

For the thermo-mechanical physical simulations of the transformation induced plasticity effects, a quenching-deformation dilatometer system DIL 805A/D+T (TA Instruments Inc.) was used. **Figure 4a** shows the principle test setup. A specimen is mounted in two grips, whereby one of them is coupled to a hydraulic system allowing tensile and compressive forces to be applied to the specimen. The specimen can be inductively heated by means of the outer coil. The integrated cooling channels in the inner coil enable the sample to be cooled with the medium helium. The dimensions of the specimens are shown in **Figure 4b**. These specimens were taken from the bulk material by means of electrical discharge machining (EDM). The experimental temperature-force-time profile is illustrated in **Figure 4c** for material 1.7225 as an example. The specimen is heated to 1000 °C with a heating rate of 50 $Ks^{-1}$ and held for a ten minutes soaking time.

Afterwards the specimen is cooled down to room temperature according to the specified cooling rate $\vartheta$. Throughout the test, the temperature is controlled by means of a type k thermocouple welded onto the specimen. Immediately before the start of the phase transformation under investigation, the force $F$ is applied and maintained until the end of the test to gain a constant load $L_F$. The change in length of the testing area from the specimen is detected via push rods and the total strain $\varepsilon^{total}$ is calculated relative to the initial length of 10 mm. The parameters of the experiments performed are listed in **Table 3**. The cooling rates of 30 $Ks^{-1}$ and 1 $Ks^{-1}$ were selected using the CCT diagrams in **Figure 3**. At these conditions, the transformation induced plasticity of the microstructural phases martensite and bainite are investigated for the material 1.7225, and the transformation induced plasticity of the microstructural phases martensite and pearlite for the material 1.3505.

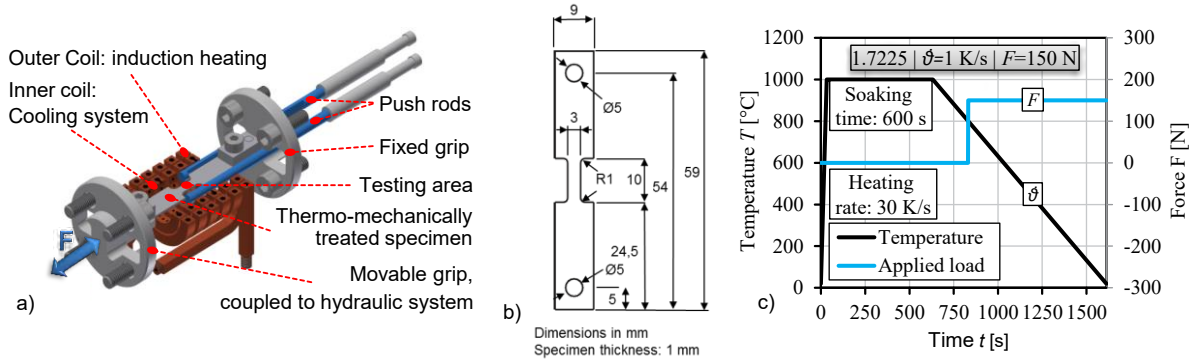


**Figure 4**: Experimental setup for analyses of TRIP effects in thermo-mechanical processes (a); dimensions of the used specimen (b) and exemplarily temperature as well as force profile of the conducted experiments.

As previous metallographic investigations of the microstructure have shown [27], these are the relevant phases which result from the cooling of the materials after hot forming for model validation in Section 3. Specifically, these microstructural phases will primarily be formed in the materials during the validation tests in Section 4. The temperature at which the load is applied was also selected for each experiment according to the CCT diagrams. The constant load $L_F$ of each experiment was varied in the tension and compression range according to the **Table 3**. The TRIP strain $\varepsilon^{tp}$ was calculated as the difference of total strain from the experiment under consideration to the total strain from a reference experiment without load, subtracting the elastic strain component due to the load. The evaluation of the total strain was in each case carried out for the specimen after cooling down to 20°C. The results of the determined TRIP strains can be found in **Table 3**. The experimental length change temperature profiles served as input data for the numerical calibration of the TRIP coefficients in Section 2.3.

**Table 3:** Parameters and results of the conducted TRIP investigations.

| **1.7225 (DIN: 42CrMo4)** | | | | **1.3505 (DIN: 100Cr6)** | | | |
|---|---|---|---|---|---|---|---|
| Cooling rate $\dot{\vartheta}$ [Ks$^{-1}$] | Onset of load [°C] | Load $L_F$ [MPa] | TRIP strain $\varepsilon^{tp}$ [%] | Cooling rate $\dot{\vartheta}$ [Ks$^{-1}$] | Onset of load [°C] | Load $L_F$ [MPa] | TRIP strain $\varepsilon^{tp}$ [%] |
| | | + 100 | + 0.45 | | | + 100 | + 0.69 |
| | | + 50 | + 0.24 | | | + 50 | + 0.32 |
| 30 | 400 | 0 | 0 | 30 | 200 | 0 | 0 |
| | | - 50 | - 0.19 | | | - 50 | - 0.23 |
| | | - 100 | - 0.38 | | | - 100 | - 0.56 |
| | | + 50 | + 0.22 | | | + 50 | - 0.2 |
| 1 | 600 | 0 | 0 | 1 | 750 | 0 | 0 |
| | | - 50 | - 0.54 | | | - 50 | - 0.29 |
| | | | | | | + tension | |
| | | | | | | - compression | |

### 2.3 Numerical study on the transformation induced plasticity

The experiments for analysis of the TRIP effects were numerically modelled in the simulation software Simufact.forming 15 based on MSC.Marc solver. The material data presented in Section 2.1 were implemented into the simulation model according to [27]. In the heat treatment module of the Simufact.forming software, a one-eighth FE-model of the test area on the used specimen was then created as shown in **Figure 5a**. The boundary conditions of the various tests from **Table 3** were defined on the basis of experimentally measured values for the temperature and load profiles. Since the exact experimental test setup can be reproduced with this FE-model, the length change temperature profiles from experiment and simulation could be compared for each test. The TRIP coefficients $K$ according to **Equation 1** were adjusted iteratively in the simulation model until the calculated curve showed a good agreement with the corresponding experimental curves. **Figure 5b** shows a comparison of the length change versus temperature curves for the material 1.7225 at a cooling rate $\dot{\vartheta} = 30$ Ks$^{-1}$ under different load conditions after adjusting the TRIP coefficient. The numerically identified values of the TRIP coefficients per microstructural phase are listed in **Table 4**. The comparison of the length change temperature profiles from the simulated and experimental TRIP tests shows that the developed material model is able to accurately consider the TRIP effect in thermo-mechanic processes under stress conditions of various directions and amounts. In Section 3, to validate the model for the residual stress calculation a hot forming process with different cooling routes is simulated.

**Table 4:** Numerically identified phase specific TRIP coefficients.

| 1.7225 (DIN: 42CrMo4) | | 1.3505 (DIN: 100Cr6) | |
|---|---|---|---|
| Phase | TRIP coefficient $K_n$ [MPa$^{-1}$] | Phase | TRIP coefficient $K_n$ [MPa$^{-1}$] |
| Martensite | $1.5444*10^{-4}$ | Martensite | $6.92011*10^{-5}$ |
| Bainite | $1.009*10^{-4}$ | Pearlite | $6.17485*10^{-5}$ |

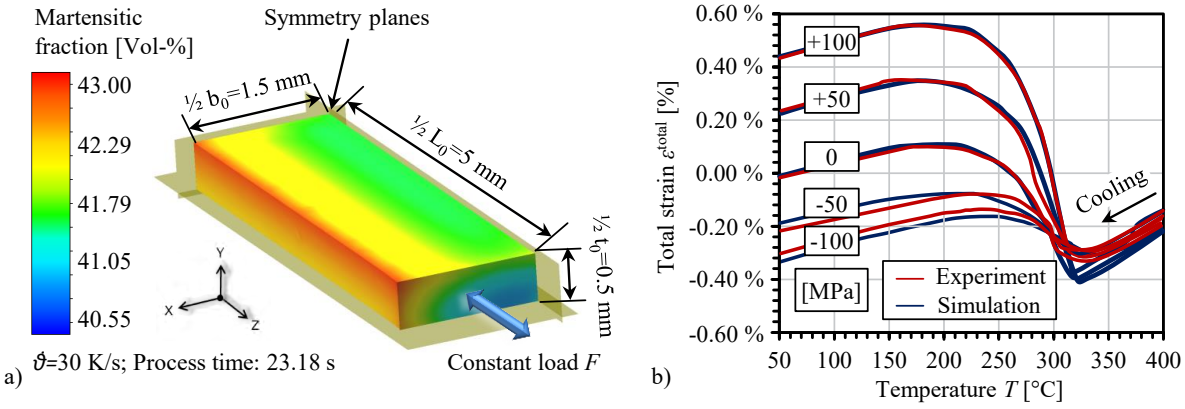


**Figure 5**: Schematics of the FE-model used for numerical study on the transformation-induced plasticity (a) and comparison of experimental and numerical longitudinal dilatations under different load scenarios (b) for 1.7225.

## 3 EXPERIMENTAL UPSETTING TESTS AND FE-MODEL VALIDATION

An experimental reference process was realized and subsequently modelled in FE simulations in order to validate the generated material models. Hereby, specimens with eccentric holes as shown in **Figure 6** are heated by an oven to the forming temperature of 1000 °C in a thermobox. After a ten minute holding time, the thermobox with the specimen including the tools is transferred to the servo-hydraulic forming simulator VHS8800 from Instron GmbH. In this way, the specimens can be compressed quasi isothermally to a final height of 28 mm at a punch speed of 200 $mms^{-1}$. Afterwards the specimens are removed from the thermobox and cooled either in water or in air. Due to the asymmetrical specimen geometry and the different cooling media, various resulting residual stresses on the surfaces of the specimens are aimed at. In order to make a sufficient statistical statement on the residual stresses resulting, the tests for both materials were carried out five times for each cooling medium. Subsequently, the tangential residual stresses $\sigma_t$ were measured on the surface at the mid-height of the specimen with an X-Ray diffractometer X3000G2 (Stresstech GmbH) according to the corresponding DIN norm [28]. As shown schematically in **Figure 8** illustrating the specimen in sectional view, there is one measuring point on the thick-walled (MP1) side and one measuring point on the thin-walled side (MP2) of the specimen. The surface of the specimen at the locus of the measuring point was electrolytically polished, in order to avoid the influence of scale layers on the measurement. The measuring point was determined by the aperture of a 2 mm collimator. Stress measurements were performed by varying the tilting area with a total of nine tilting positions. Afterwards the measurements were evaluated with the software XTronic (Stresstech GmbH).

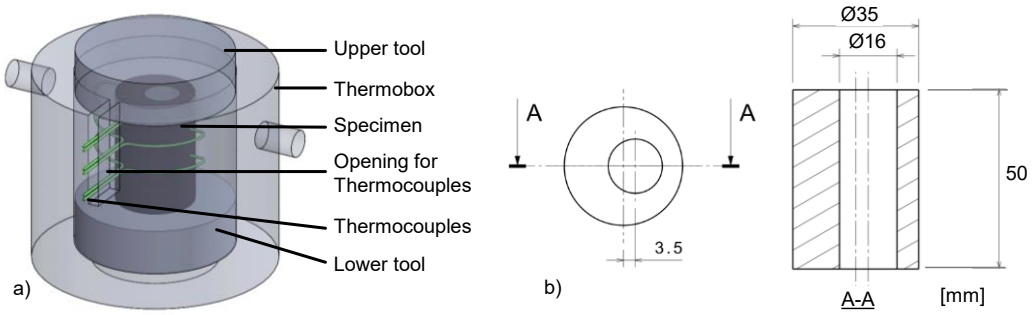


**Figure 6**: Principal representation of the specimen prepared with thermocouples in the thermobox (a) and shape of the investigated specimen with dimensions in mm (b).

The previously described thermo-mechanical cylinder upsetting tests were numerically modelled with the commercial FE software Simufact.forming 15 based on MSC.Marc solver. When heated to 1000 °C, a homogeneous austenitic structure is formed in the materials, whereby the previously existing residual stresses are almost completely dissolved. From this point on, a new residual stress profile can be generated by the thermo-mechanical forming process. Accordingly, the process simulation is started with a thermally expanded workpiece at 1000 °C with the initial condition of a 100% austenitic microstructure. The FE-model for the simulation of the reference process including the boundary conditions is shown in **Figure 7**. The tools are considered as heat conducting rigid bodies and provided with a mesh of 1 mm element edge length. For the tools of the material 2.4668 (DIN: NiCr19NbMo) constant values of the specific heat capacity $c_p = 435$ J/kgK and heat conductivity $\lambda = 11.4$ $Wm^{-1}K^{-1}$

were taken from the data of the supplier [29]. The workpiece is assigned with an adaptive hexagonal mesh with the minimum element edge length of 0.5 mm, which was determined in a mesh sensitivity analysis. The simulation model consists in total of 56500 hex elements for the tools and 24000 hex elements of the workpiece.

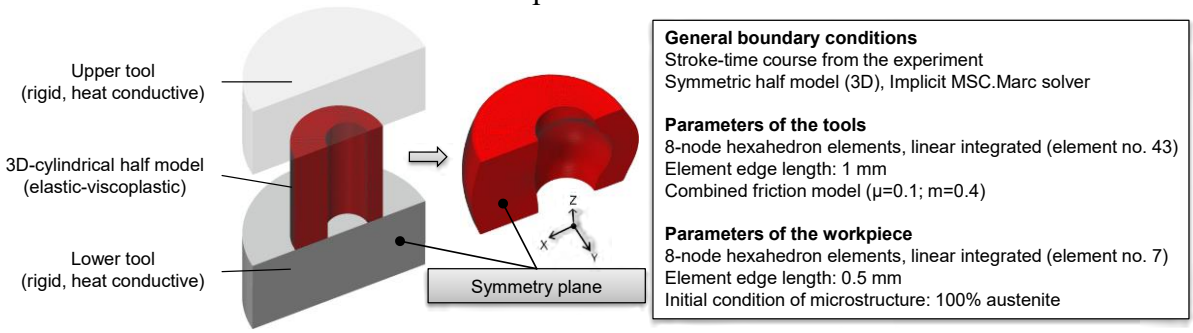


**Figure 7:** Design of the investigated FE-simulation model and the boundary conditions.

The results of the FE-simulations were compared with the experimentally measured residual stress values. As can be seen in the **Figure 8a** and **b**, the residual stresses due to rapid cooling in water are higher than those after cooling in air. For cooling in water, 1.7225 tangential residual stresses of $\sigma_t$=212 MPa at MP1 and $\sigma_t$=192 MPa at MP2 were determined. The stresses resulting from the cooling in air are $\sigma_t$=27 MPa at MP1 and $\sigma_t$=19 MPa at MP2. The residual stresses $\sigma_t$=216 MPa for MP1 and $\sigma_t$=138 MPa for MP2 during cooling in water were measured on the specimens of the material 1.3505. After cooling in air, compressive residual stresses of $\sigma_t$=-83 MPa were measured for MP1 and $\sigma_t$=-52 MPa for MP2. At high cooling rates, a diffusion-free transformation of the austenitic into the martensitic phases takes place in the material, which leads to severe stresses in the crystal lattice. During diffusion-controlled phase transformation, which occurs during cooling in air, comparatively lower residual stresses in the range of zero can be observed.

The comparison of the experimentally measured residual stresses and the values obtained from simulations shows that the developed FE-model was suitable for a good prediction accuracy of the residual stresses. In particular, the differences in the amount of residual stresses during cooling in the water between the thick-walled side (MP1) and the thin-walled side (MP2) of the specimen were calculated properly in the simulations. In order to further improve the simulation model, the TRIP coefficients could be identified in additional studies both temperature and load dependent.

With this experimental reference test of hot forming the developed FE simulation model could be validated for different cooling conditions at different measuring points of the specimen with eccentric hole.

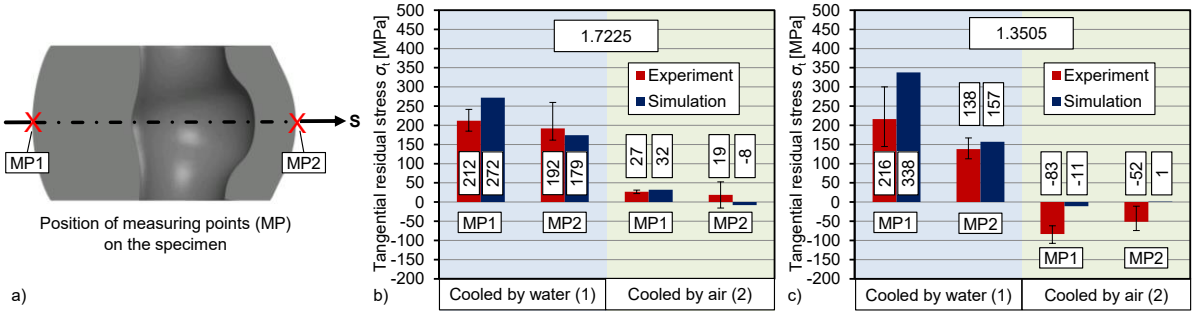


**Figure 8:** Positions for residual stress evaluation on the principally depicted sectional view of the thermo-mechanically processed specimen (a) as well as results from experiements and simulations for 1.7225 (b) and 1.3505 (c).

## 4 SUMMARY AND OUTLOOK

In this work material models as well as simulation methods for the calculation of residual stresses in a hot forming process with different cooling routes were developed. In order to characterise the TRIP effect in the considered materials 1.7225 and 1.3505, TRIP coefficients were determined using an experimental-numerical approach and implemented in the FE-model. A simplified hot forming process for the investigation of the residual stress development, using cylindrical specimens with eccentric holes, was experimentally realised and subsequently residual stress measurements on the specimen surfaces were performed using X-ray diffraction. These measurements finally led to validation of the developed FE-models.

In a next step, the influences of the residual stresses of the second and third type from the microscale on the macroscopic residual stresses are to be investigated using multi-scale simulation approaches. In this way, new insights into the effects of the local stress gradients in the component can be gathered and the simulations can then be further improved. Finally, the developed FE-models are to be verified in the context of an industrial forging process.

**Acknowledgement**

Funded by the Deutsche Forschungsgemeinschaft (DFG, German Research Foundation) - 374871564 (BE 1691/223-1) within the priority program SPP 2013.

## REFERENCES

[1] Verlinden B, Driver J, Samajdar J and Doherty RD, 2007. Thermo-mechanical processing of metallic materials, Elsevier Science 11, ISBN: 9780080444970.

[2] Brands, D.; Chugreev, A.; Kock, C.; Niekamp, R.; Scheunemann, L.; Uebing, S.; Behrens, B.-A.; Schröder, J., 2018. On the analysis of microstructural residual stresses in hot bulk forming parts under specific cooling. Proc. Appl. Math. Mech., 18: e201800256.

[3] Behrens, B.-A.; Bouguecha, A.; Vucetic, M.; Chugreev, A., 2016. Advanced Wear Simulation for Bulk Metal Forming Processes, MATEC Web of Conferences, 80, 04003, DOI: http://dx.doi.org/10.1051/matecconf/20168004003.

[4] Behrens, B.-A., Olle, P., 2007. Consideration of phase transformations in numerical simulation of press hardening. Steel Research International, 78 (10-11), 784-790.

[5] Behrens, B.A.; Bouguecha, A.; Bonk, C.; Chugreev, A., 2017. Experimental investigations on the transformation induced plasticity in a high tensile steel under varying thermo-mechanical loading, Computer Methods in Materials Science 17 (1), 36-43.
[6] Behrens, B.-A.; Chugreeva, A.; Chugreev, A., 2018. FE-simulation of hot forging with an integrated heat treatment with the objective of residual stress prediction. AIP Conference Proceedings, 1960 (1), 040003, DOI: https://doi.org/10.1063/1.5034857.
[7] Denis, S.; Gautier, E.; Simon, A.; Beck, G., 1985. Stress-phase-transformation interactions - basic principles, modelling and calculation of internal stresses. Materials Science and Technology, 1, 805–814.
[8] Mitter, W., 1987. Umwandlungsplastizität und ihre Berücksichtigung bei der Berechnung von Eigenspannungen; Vol. 7, Materialkundlich-Technische Reihe, Gebrüder Bornträger Verlag, Berlin.
[9] Behrens, B.-A.; Bach, Fr.-W.; Bouguecha, A.; Nürnberger, F.; Schaper, M.; Yu, Z.; Klassen, A, 2012. Numerical calculation of an integrated heat-treatment process for precision forged parts. Journal of Heat Treatment and Materials, 67 (5), 337-343.
[10] Besserdich, G., 1993. Untersuchungen zur Eigenspannungs- und Verzugsbildung beim Abschrecken von Zylindern aus den Stählen 42CrMo4 und Ck45 unter Berücksichtigung der Umwandlungsplastizität. Dissertation, Universität Karlsruhe.
[11] Gautier, E.; Simon, A.; Beck, G.: Deformation of eutectoid steel during pearlitic transformation under tensile stress. In: Strength of metals and alloys. Proc. 6th Int. Conf., ICSMA 5, 27.-31.8.1979 in Aachen, 2, S. 867-873.
[12] Mahnken, R., Schneidt, A., Antretter, T., 2009. Macro modelling and homogenization for transformation induced plasticity of a low-alloy steel. Int. J. Plast., 25 (2), 183-204.
[13] Lütjens, J., Hunkel, M., 2013. □e in□uence of the transformation plasticity effect on the simulation of partial press-hardening, HTM J. Heat Treatm. Mat., 68 (4), 171-177.
[14] Leblond, J.B., 1989. Mathematical modelling of Transformation Plasticity in Steel II. Coupling with strain hardening phenomena, Int. J. Plast., 5 (6), 573-591.
[15] Böhm M., Wolff M., 2003. Umwandlungsplastizität bei Stählen im Konzept der Thermoelasto-Plastizität. J. Mech. Phys. Solids, 29-48.
[16] Fischer F. D., Sun Q. P., Tanaka K., 1996. Transformation-induced plasticity (TRIP). Appl. Mech. Rev., 49, 317-364.
[17] Turetta A., Ghiotti A., Bruschi S., 2007. Investigation of 22MnB5 mechanical and phase transformation behaviour at high temperature. Proceedings of IDDRG-conference, 147-153.
[18] Behrens, B.-A.; Bouguecha, A.; Bonk, C.; Chugreev, A., 2017. Numerical and experimental investigations of the anisotropic transformation strains during martensitic transformation in a low alloy Cr-Mo steel 42CrMo4. Proc. Eng., 207, 1815–1820.
[19] DIN EN 10083-3 (2007) Steels for quenching and tempering – Part 3: Technical delivery conditions for alloy steels, Beuth-Verlag.
[20] DIN EN ISO 683-17 (2014) Heat-treated steels, alloy steels and free-cutting steels – Part 17: Ball and roller bearing steels, Beuth-Verlag.
[21] Hensel A.; Spittel T, 1978. Kraft- und Arbeitsbedarf bildsamer Formgebungsverfahren; Deutscher Verlag für 542 Grundstoffindustrie.
[22] Behrens B.A.; Chugreev A.; Kock, C., 2018. Experimental-numerical approach to efficient TTT-generation for simulation of phase transformations in thermomechanical

forming processes. IOP Conference Series, Materials Science and Engineering, 461, 012040.

[23] Acht C., Dalgic M., Frerichs F., Hunkel H., Irretier A., Lübben T., Surm H., 2008. Ermittlung der Materialdaten zur Simulation des Durchhärtens von Komponenten aus 100Cr6. Journal of Heat Treatment and Materials, 63, 234–244.

[24] JMatPro. Practical software for materials properties, https://www.sentesoftware.co.uk/jmatpro, 2018.

[25] Saunders N., Guo U.K.Z., Li X., Miodownik A.P., Schillé J.P, 2003. Using JMatPro to Model Materials Properties and Behavior. JOM, 55, 60–65.

[26] Guo Z., Saunders N., Schillé J.P., Miodownik A.P, 2009. Material properties for process simulation. Materials Science and Engineering: A 1-2, 7–13.

[27] Behrens B.-A., Schröder J., Brands D., Scheunemann L., Niekamp R., Chugreev A., Sarhil M., Uebing S., Kock C, 2019. Experimental and numerical investigations on the development of residual stresses in thermo-mechanically processed Cr-alloyed steel 1.3505. Metals, 9(4), 480, DOI: https://doi.org/10.3390/met9040480

[28] DIN EN 15305:2009-1, Non-destructive testing - Test method for residual stress analysis by X-ray diffraction, Beuth Verlag, 2008

[29] Special Metals Co.. New Hartford, New York, USA, http://www.specialmetals.com/assets/smc/540 documents/pcc-8064-sm-alloy-handbook-v04.pdf, 2018.